Shock-Shock Interaction and its Significance in Hypersonic Vehicle Design

Benjamin S. Kirk
The University of Texas at Austin
Austin, Texas 78712
benkirk@cfdlab.ae.utexas.edu

Presented to:
Dr. David Dolling
ASE 382R – Hypersonic Aerodynamics

February 17, 2005

Abstract

This paper reviews the phenomenon of shock–shock interaction in compressible flows and focuses in particular on the influence this phenomenon has on hypersonic vehicle design. Interest in the problem is motivated though a historical overview and review of previous work. State–of–the–art techniques employed by researchers in studying the shock–shock interaction problem are also critically reviewed. The impact of the shock–shock interaction problem on existing and future hypersonic vehicle designs is then considered. The general conclusion is that the shock–shock interaction phenomenon is both very difficult to predict accurately and an absolutely critical component of hypersonic vehicle design for a number of technical reasons. At the same time the importance of this phenomenon will become increasingly important as the aerospace industry seeks to create more efficient designs, thus a detailed understanding of this phenomenon is required for the development of next–generation flight vehicles.

Contents

List of Figures

1 Introduction

Shock–shock interaction (SSI) is a physical phenomenon that occurs when multiple shock waves in a compressible flowfield intersect and interact in some way. When such interactions occur very complicated and localized aerothermodynamic processes may result which can influence a supersonic vehicle by creating regions of intense heating (easily an order of magnitude higher than in the case of undisturbed flow) or extremely high pressure loads. In general, the intensity of these interactions becomes more severe in hypersonic flight regimes. Additionally, analysis of SSI effects on a vehicle that operates in the hypersonic regime can be complicated by the presence of real gas effects.

Historical examples of hypersonic flight vehicles such as the X-15 rocket plane and Space Shuttle Orbiter indicate that the consequences of not accounting for SSI effects in vehicle design can be severe. Indeed, in hypersonic flight regimes SSI effects can easily cause complete vehicle failure if not accounted for in the vehicle design phase. As modern trends in aerospace technology focus on reusable, efficient hypersonic vehicles the role SSI effects play in vehicle design becomes even more pronounced.

A literature review illustrates that little thought was given to the SSI interaction problem until the end of the 1960's. Since that time a significant amount of work has led to a basic understanding of the problem that will presented in the following sections. However, what is interesting about the SSI phenomenon is that when compiling a list of factors important in the accurate prediction of SSI effects we find that our list includes nearly all of the current "research phenomenon" in high speed fluid dynamics. These phenomenon include (but are certainly not limited to):

- Real gas effects in hypersonic flight regimes
- Shear layer/boundary layer instability and transition
- Shock Wave/boundary layer interaction
- Adequate shock wave resolution in computational models
- Accurate convective heat transfer rate measurement and prediction

It is thus safe to say that the SSI problem will not be "solved" in any meaningful way in the foreseeable future.

2 Problem Motivation

Little was known about the SSI phenomenon prior to the X-15 flight program that took place in the 1960's. Although some researchers had investigated SSI phenomenon experimentally, most of the existing work lacked the resolution necessary to measure peak heat fluxes and pressure loads in interaction regions. The reason for this is rather simple: the interaction regions tend to be very localized and researchers had no reason to expect extremely high, localized loads.

Thus when analyzing experimental data relatively benign increases in heat and pressure loads seemed reasonable, and the researchers had no reason to study the problem in more detail.

In retrospect we see that the early pioneers of SSI research were missing the fine–scale phenomenon that make this interaction such a critical (and potentially catastrophic) phenomenon. We now know that in certain types of interaction patterns peak heat and pressure loads can easily be *an order of magnitude* higher than in similar, non–interacting flow. In certain cases even higher loads will occur. With this in mind it is clear that the success or failure of a vehicle operating in the hypersonic regime will depend on whether or not the SSI problem was properly addressed during the design phase. This is not an exaggeration. Accounting for SSI effects in vehicle design will not simply effect the efficiency of the design, but rather will dictate whether the vehicle burns up or operates as intended in the hypersonic regime. To further illustrate the importance SSI effects can play in vehicle performance it is useful to consider a historical example.

2.1 Historical Example: The X-15 Leading Edge

NASA developed the X-15 experimental rocket plane in the late 1950's. The plane was designed to be jettisoned at altitude from under the wing of a modified B-52 bomber. The rocket motor would then ignite and accelerate the aircraft to a maximum speed of Mach 6.7 at a peak altitude of 67.1 miles. In this flight regime we can expect the influence of aerodynamic heating on the vehicle to be significant [8]. The first X-15 flight took place on June 8, 1959, and the three aircraft built logged a total of 199 flights before the program ended in November 1968 [9]. The X-15 program provided a tremendous amount of data about flight in the hypersonic regime. Much of this data would be indispensable in the subsequent design of the Space Shuttle.

One of the consequences of hypersonic flight is increasingly swept shock waves. Figure 1 clearly illustrates this point. The image on the left depicts the shock

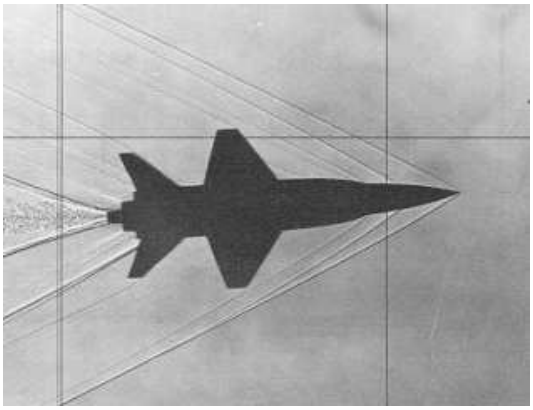

(a) $M_\infty = 3$

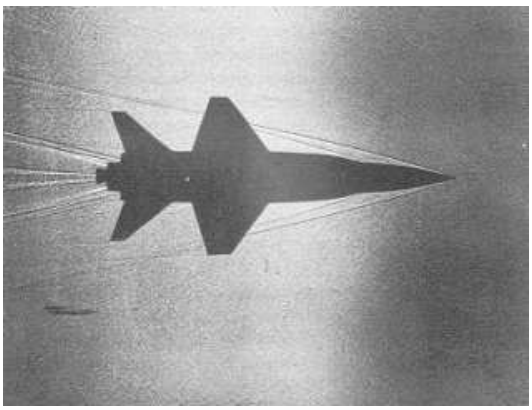

(b) $M_\infty = 6$

Figure 1: X-15 WIND TUNNEL TESTS AT $M_\infty = 3$ AND $M_\infty = 6$

structure around the X-15 at $M_\infty = 3$, and the image on the right corresponds to $M_\infty = 6$. The interesting feature of the Mach 6 case is that the oblique shocks formed by the nose and canopy are considerably more swept than in the Mach 3 case. In fact, the image clearly illustrates that the nose and canopy shocks are sufficiently swept that they intersect the wings of the vehicle. This has two consequences for the design that are worth noting:

- Different sections of the wing see markedly different flow conditions
- The nose and canopy shocks will impinge on the wings and may interact with leading–edge shocks

It is this second point that is of interest with respect to the SSI phenomenon.

For certain flights the X-15 was modified with the addition of an ablative coating. Figure 2 shows one of these vehicles immediately after being dropped from a B-52. This particular X-15 has also been modified with the addition of two external fuel tanks and a dummy ramjet engine fixed to the lower tail fin. The ablative coating was added to enable higher speed flight by admitting higher

Figure 2: X-15 WITH ABLATIVE COATING IN FLIGHT [1]

surface temperatures. The coating responds to a high heating environment by charring and actually burning away, thus removing energy that would otherwise be transferred to the vehicle. After a flight areas of intense heating can thus be observed by locating regions of charred coating. Figure 3 depicts the wing and its coating after a flight. Areas of charring (caused by high heat loads) are evident on the leading edge of the wing in the region of nose shock/leading edge shock

interaction. This clearly illustrates that there is a phenomenon associated with the interaction that is causing high heat loads.

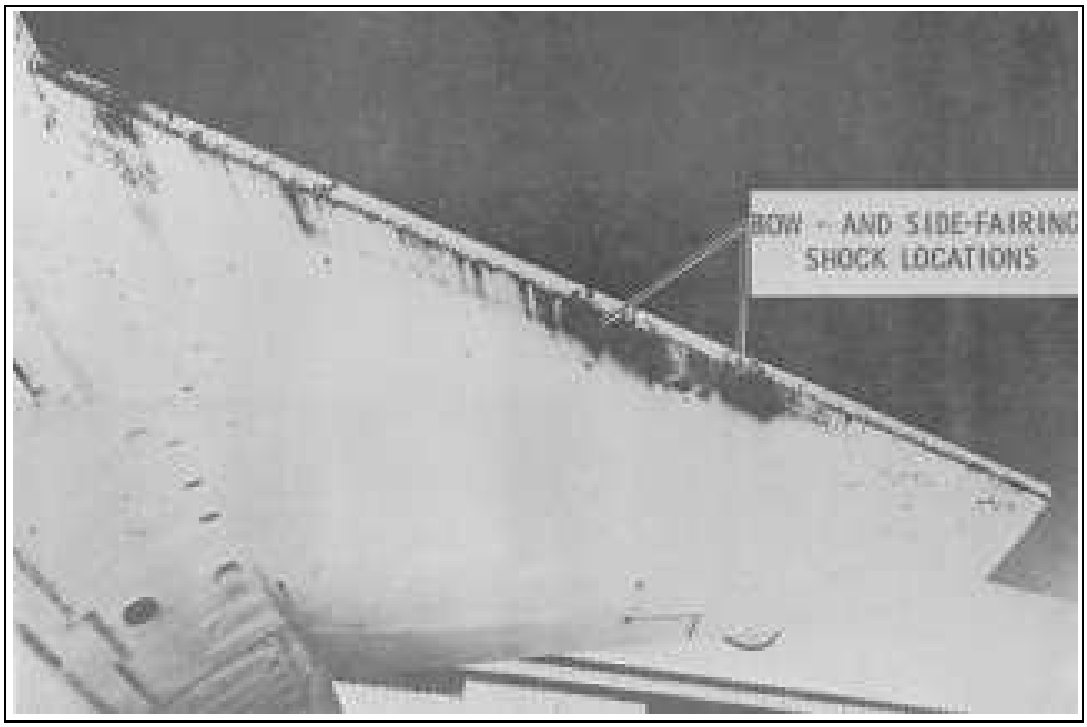

Figure 3: Charred leading edge due to nose shock/wing shock interaction [1]

2.2 Historical Example: The X-15 Ramjet Experiment

An even more extreme example of the effect SSI can have in the hypersonic regime is illustrated by considering the ill-fated X-15 ramjet experiment. In this experiment a dummy ramjet was instrumented and attached to X-15's lower fin. The configuration is shown in Figure 4. The setup was to be tested at Mach 6 in order to provide data for later ramjet design refinement. Prior to landing the pilot, Peter Knight, was to explosively jettison the ramjet so that the X-15 could land uninhibited [3].

The test flight took place on October 3, 1967. The flight proceeded as planned. During the flight the aircraft reached a peak speed of Mach 6.72. At the end of the flight Knight completed the jettison procedure and landed without incident. Post-flight interviews with Knight indicated that he thought the flight had proceeded normally until he landed. At that time the ground crew rushed to the rear of the plane. Since they usually would have helped him out of the craft, Knight immediately knew something was amiss [3].

Figure 5 shows the lower tail fin after the flight. It turns out that while Knight thought the flight was normal, the bottom fin of his craft had actually melted away. Post-flight analysis indicated that several of the explosive bolts failed during the flight when extreme temperatures in the fin-ramjet attachment region

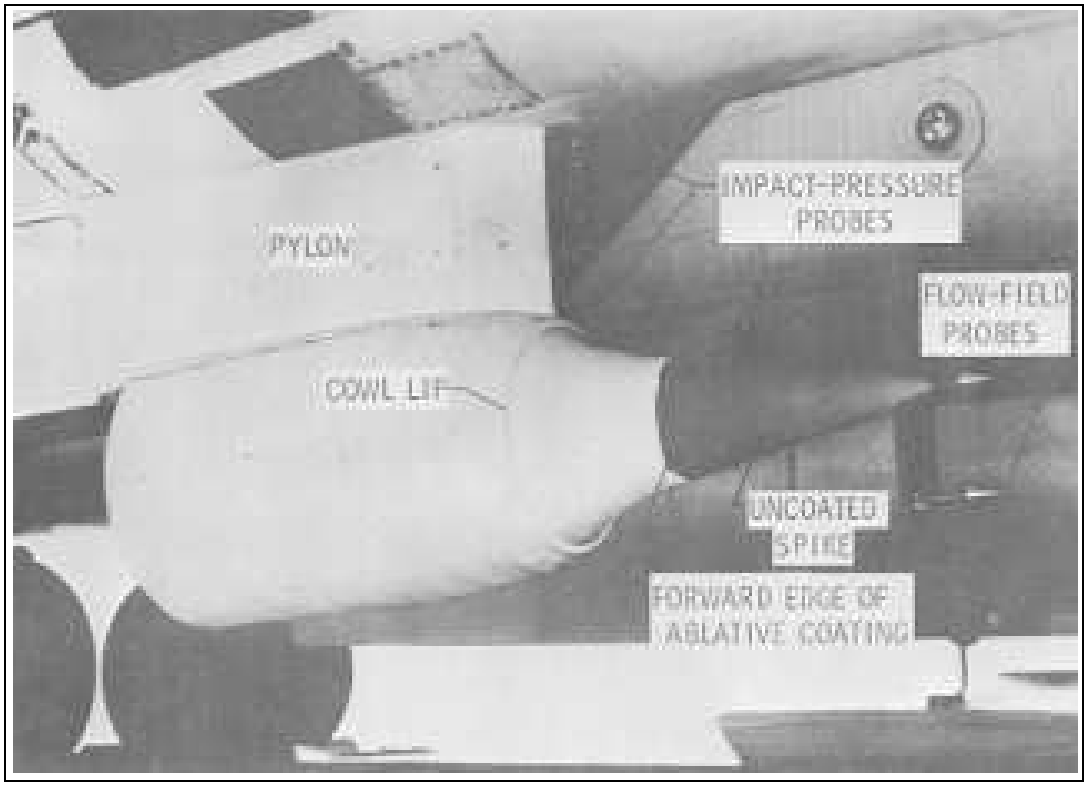

Figure 4: Dummy ramjet attached to the X-15's lower fin [2]

occurred. Analysis suggested that when this happened the remaining attachment points failed due to shear loads and the ramjet fell away from the vehicle. Thermal analysis indicated that the fin was subjected to heat fluxes approximately *seven times* higher than those the vehicle was designed to withstand. The cause of the structural failure was eventually attributed to SSI. At Mach 6 a swept conical shock was formed from the nose of the ramjet. This shock then interacted with the bow shock created by the X-15's lower fin [3]. What none of the engineers realized before the flight was that the resulting heating environment would be as severe as it actually was. It is actually quite fortunate that the damage to the lower fin did not adversely effect the vehicle aerodynamics in such a way that Knight lost control of the aircraft at Mach 6. Had that occurred both the aircraft and the pilot could have been lost.

An interesting fact related to this incident is that the dummy ramjet was successfully recovered despite being ripped away from the vehicle at high altitude. Analysis of the telemetry data indicated an instantaneous decrease in drag on the vehicle. Flight engineers correctly associated this drag reduction with the loss of the ramjet engine. The initial conditions for a ballistic trajectory analysis were then determined from the flight conditions. The engineers estimated the location of the ramjet and successfully located it on the Edwards Air Force base bombing range [3].

A literature review shows that prior to the X-15 ramjet failure there had been

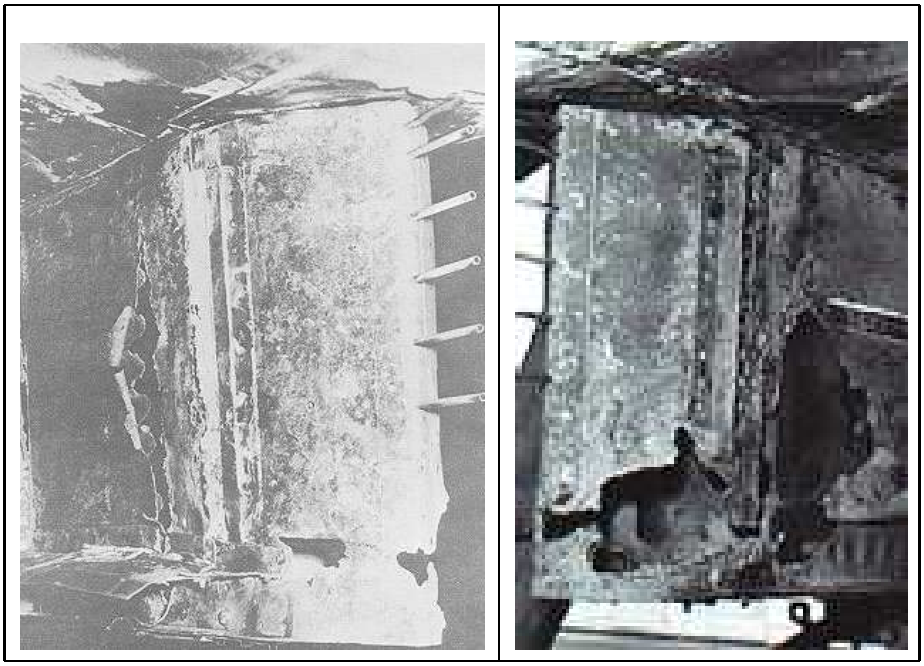

Figure 5: X-15 LOWER FIN DAMAGE CAUSED BY SSI [3]

little research related to the SSI phenomenon. This incident understandably motivated an intense amount of interest in SSI. It is quite fortunate that this first experience with the SSI phenomenon was relatively benign. Engineers were thus alerted to the SSI problem and began considering it in the design of hypersonic vehicles. Had this failure not occurred on the X-15 it is conceivable that SSI could have caused a more catastrophic failure on some other vehicle at a later time.

3 A Closer Look at the SSI Problem

3.1 First Investigations of SSI

It has been mentioned that there was little experimental research related to the SSI problem prior to the X-15 ramjet experiment failure in 1967. At that point the work of Francis [10], Heirs & Loubsky [11], and Newlander [12] were some of the only experimental results that examined the effect the SSI problem had on heat transfer rates to a body. These works generally examined swept cylinders in a variety of flowfields. Unfortunately, many of these early investigators expected boundary layer transition in the vicinity of the interaction region to be the cause of locally increased heating rates. They were thus often overly concerned with details of the boundary layer and did not focus enough attention on the effect of the shock interaction patterns in experiments. The extensive work by Edney [4] was the first in–depth experimental research that considered the effect of various shock interaction patterns on a number of geometries.

3.2 Edney's Approach

Edney examined a number of glass models in a Mach 4.6 wind tunnel. The models were instrumented with platinum thin–film gages that were used to measure heat transfer rates. These gages were connected to an analog circuit network that allowed Edney to calibrate and measure the surface heat flux. An oscilloscope was used to visualize the heating distribution around the glass models that these gages recorded. Static ports and a quasi–static injection technique was used to measure the static pressure distribution on the model surface.

The general setup Edney used is illustrated in Figure 6. The flow direction in the figure is from left to right. A flat plate with a slot cut through it was placed in the test section of the wind tunnel. The tunnel was started and an

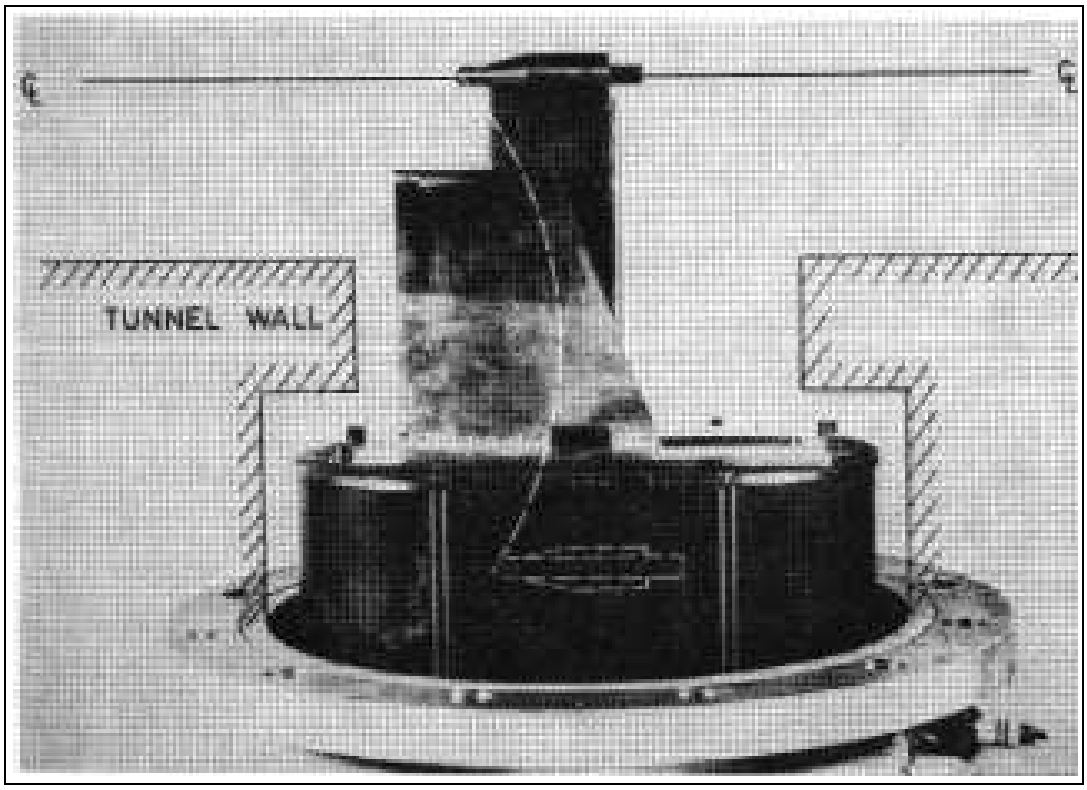

Figure 6: Edney's experimental setup used to study SSI [4]

oblique shock of known strength developed from the leading edge of this plate. The model, which was mounted on a sting, was then injected into the flowfield through the slot in the flat plate. As the model entered the flowfield it passed through the boundary layer associated with the tunnel wall, though the plate boundary layer, and finally came to rest in such a way that the oblique shock formed by the flat plate interacted with the bow shock created by the model.

In this way Edney was able to accurately measure the heat flux and pressure loads on the surface of the model that resulted. Edney was able to adjust the plate angle to obtain oblique shocks of various strength and angle. He tested hemispheres, cylinders, and wedge–shaped models in [4].

3.3 Edney's Results

Edney's research demonstrated that severe heat flux and pressure loads can occur in flowfields where shock–shock interaction is important. In some instances he found that the peak heat transfer rate to a vehicle could be *an order of magnitude* or more higher than the rate that would result in a flowfield without shock interaction. This was not a particularly surprising result in the light of what had recently happened during the X-15 ramjet experiment, however Edney was apparently the first person to measure these intense, localized heat loads experimentally. His results indicated that the region of peak heat flux in a SSI–induced flowfield could be quite small, so adequate resolution was critical in observing this phenomenon experimentally. His results also suggested that it was this lack of resolution that caused these severe heating environments to be missed in previous experiments [4].

Edney identified six distinct interaction patterns that result from SSI. These different interaction patterns will be discussed in detail in the following sections. He also identified four key factors (neglecting transition and turbulence effects) that dictate the pattern that results. These parameters include:

- Freestream Mach Number
- Geometry
- Strength of the Impinging Shock
- Location of the Impinging Shock

Edney also developed analytical methods of analyzing these various interaction patterns. These models clearly illustrated that real gas effects (in particular the variation of γ, the ratio of specific heats) play an extremely important role in determining the peak pressure loads and heat flux in an interaction region [4]. This importance of real gas effects is one of the factors that complicates the analysis of SSI in the hypersonic flow regime.

3.3.1 Type I Interaction

The type I interaction pattern is shown schematically in the top of Figure 7. In the lower part of the figure a type I interaction created by a wedge and a swept cylinder are illustrated. This interaction pattern results when the impinging shock impinges on the bow shock in a region well beyond the lower sonic line of the bow shock. The resulting flow in regions 3 and 4 of the schematic diagram thus supersonic. A shear layer develops at the impingement point and is convected downstream, away from the body. The shear layer is thus unlikely to effect the heat transfer to the vehicle.

The impinging shock is transmitted through the bow shock and continues on toward the body (shown schematically as line PR). This shock may then impact the body and cause boundary layer separation/reattachment or induce transition and turbulence. These effects will generally increase the wall heat transfer rate [4]. Indeed the flow visualization in the bottom of the figure shows

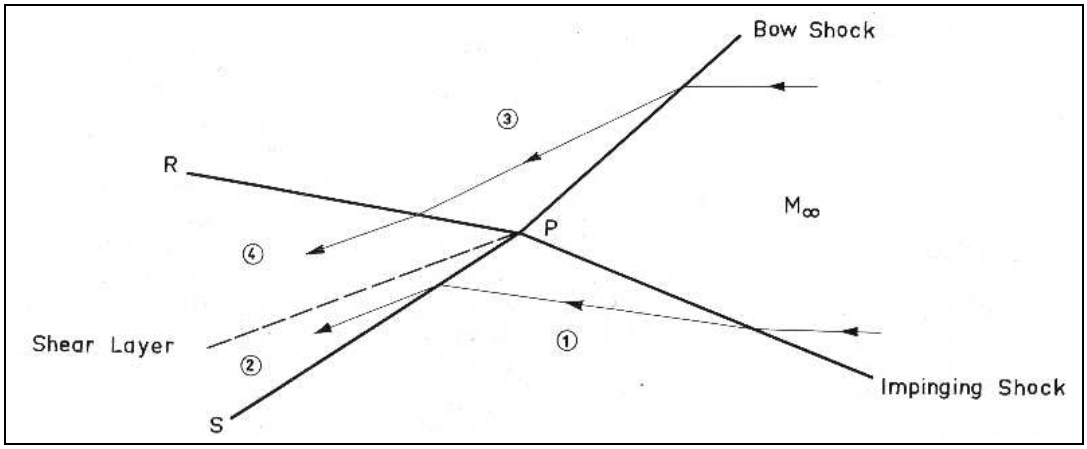

(a) Schematic Diagram

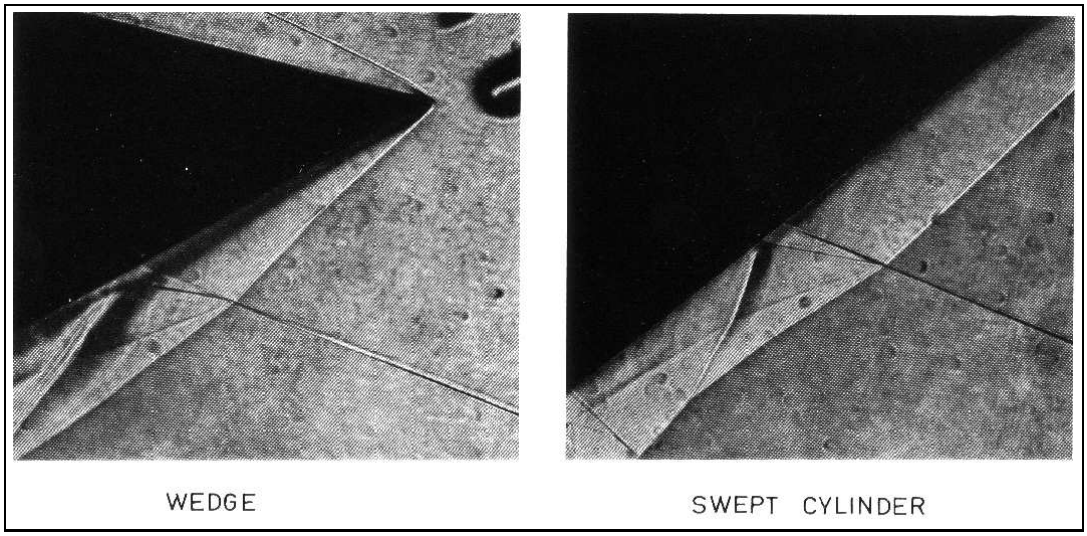

(b) Image from Edney's Experiment

Figure 7: Type I Interaction [4]

that this shock does hit the body and is reflected. Due to the adverse pressure gradients introduced by the shock–body intersection it would not be unreasonable to expect boundary layer separation to occur near the shock–body impingement point.

3.3.2 Type II Interaction

The type II interaction pattern is shown in Figure 8. This pattern occurs when the impinging oblique shock interacts just below the lower sonic line of the bow shock created by the body. A characteristic feature of this interaction pattern is the strong normal shock illustrated schematically by line PQ. Behind this shock a subsonic region surrounded by two shear layers results. The width of this subsonic region is found to be dependent on the particular body that causes the interaction. The shear layer that emanates from point P is the stronger of

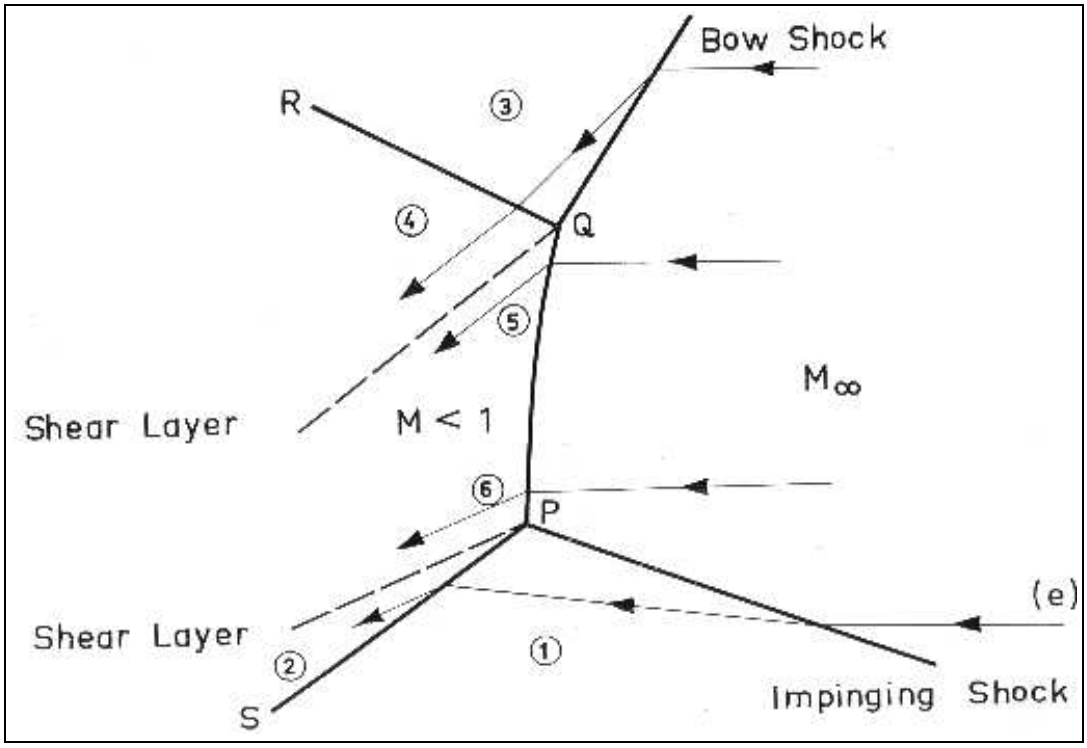

(a) Schematic Diagram

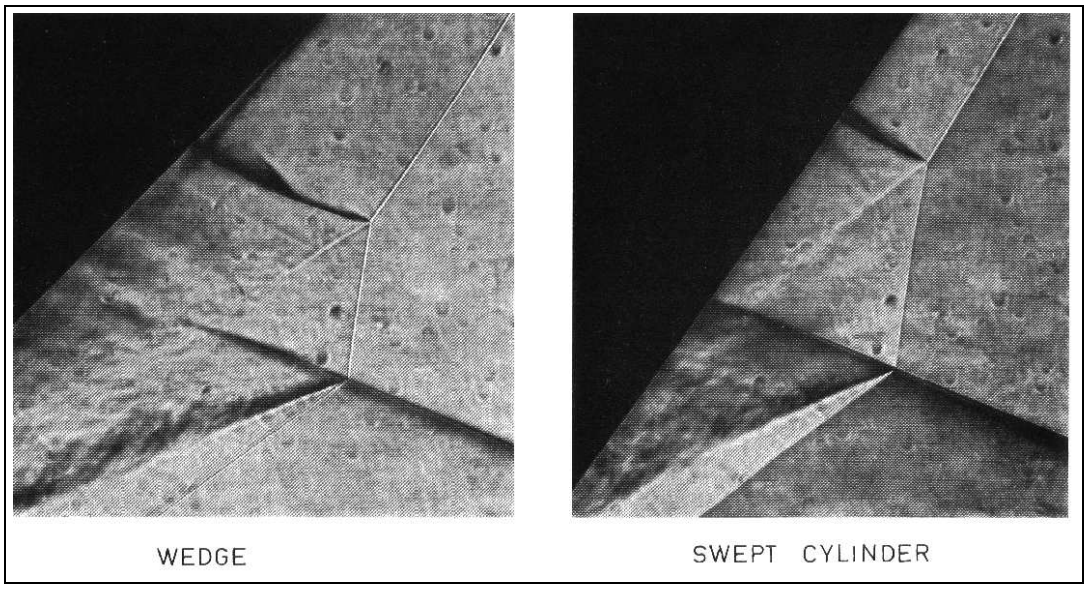

(b) Image from Edney's Experiment

Figure 8: Type II Interaction [4]

the two shear layers, as suggested by the flow visualization images. The heat transfer rate to the body can increase significantly if this strong layer comes in contact with the surface. Additionally, the layer is observed to travel a significant distance before it impacts the body and thus may very well be transitional or turbulent, which could also lead to local increases in heat transfer.

The shock illustrated in the schematic as line QR will continue on until it hits the body. In the visualization images this shock is seen to impact the body at nearly a 90° angle, and thus the boundary layer will see a strong, nearly normal shock and an associated large adverse pressure gradient, which is likely to induce separation. It is difficult to determine conclusively from the still images, but it appears that a shock–boundary layer instability results from this interaction. The region where QR intersects the body is not a distinct line like we might expect for a steady shock wave but is a rather blurry region. This fact and the periodic variations downstream of the interaction region in the case of the wedge suggest that the shock–boundary layer interaction is unstable and is causing temporal variations in the flowfield. It would not be surprising to find increased heat loads in the region of this unsteady interaction if the boundary layer is indeed separating and reattaching in a periodic manner. Current work by Dolling [13] illustrates that the shock wave–boundary layer interaction problem is difficult in its own right, so we can expect the analysis of SSI patterns that induce this effect to be even more difficult.

3.3.3 Type III Interaction

The type III interaction pattern is shown in Figure 9. This interaction pattern occurs when the impinging shock hits the body bow shock inside the subsonic region near the front of the body. Since the flow behind the bow shock is subsonic in this interaction the impinging shock cannot be transmitted to the body surface. However, a strong shear layer PR develops over a fairly large region and will later attach to the surface of the body. Accordingly, the shear layer may be fully turbulent by the time it reattaches at point R.

This reattachment is further complicated by the nearly normal shock QR that intersects the body. The general effect of the pressure rise caused by this shock is to thin the boundary layer. This will increase the convective heat transfer rate by increasing the temperature gradients that occur at the wall. This problem may be complicated by the attaching shear layer, which may be laminar or turbulent [4].

An interesting feature of the type III interaction pattern is that much of its behavior can be examined by looking to existing research on the attaching shear layer problem. Attaching shear layers are a common phenomenon and have been studied fairly extensively by Finley [14], Baker & Martin [15], and others. Thus in the case of the type III interaction an important feature of the SSI flowfield can be analyzed using existing research. Analysis of the attaching shear layer problem does suggest that locally increased heating rates will result, so the type III interaction must be carefully considered in vehicle design.

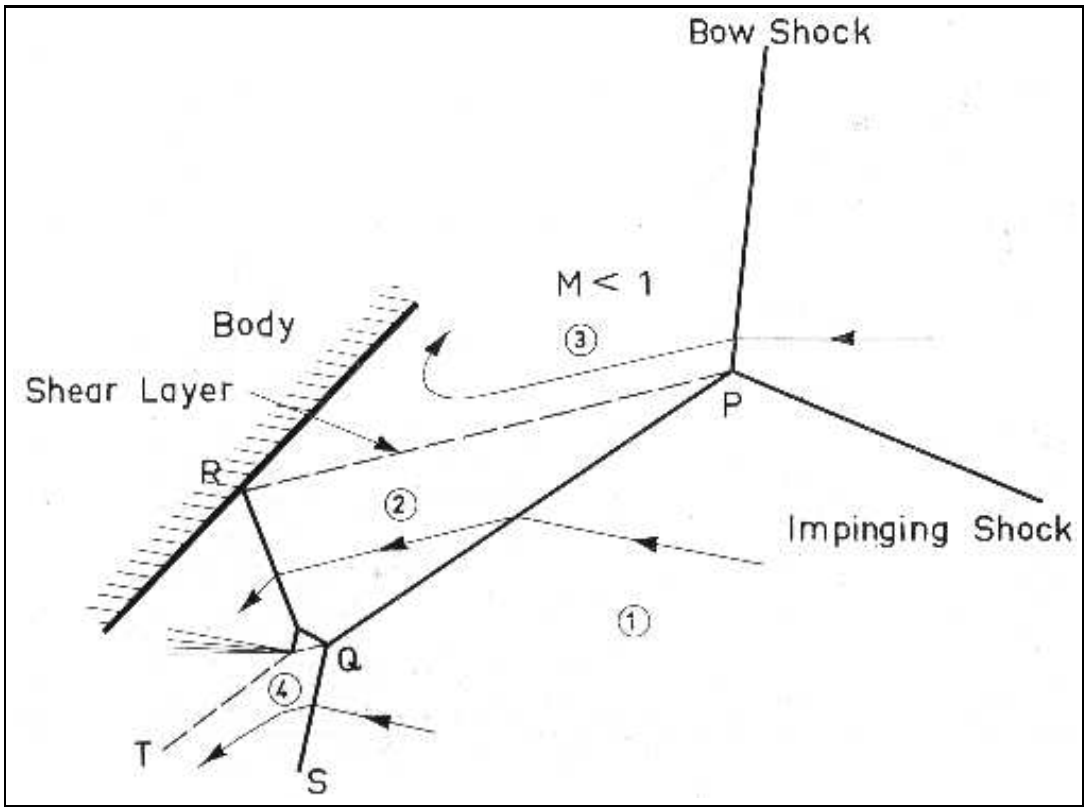

(a) Schematic Diagram

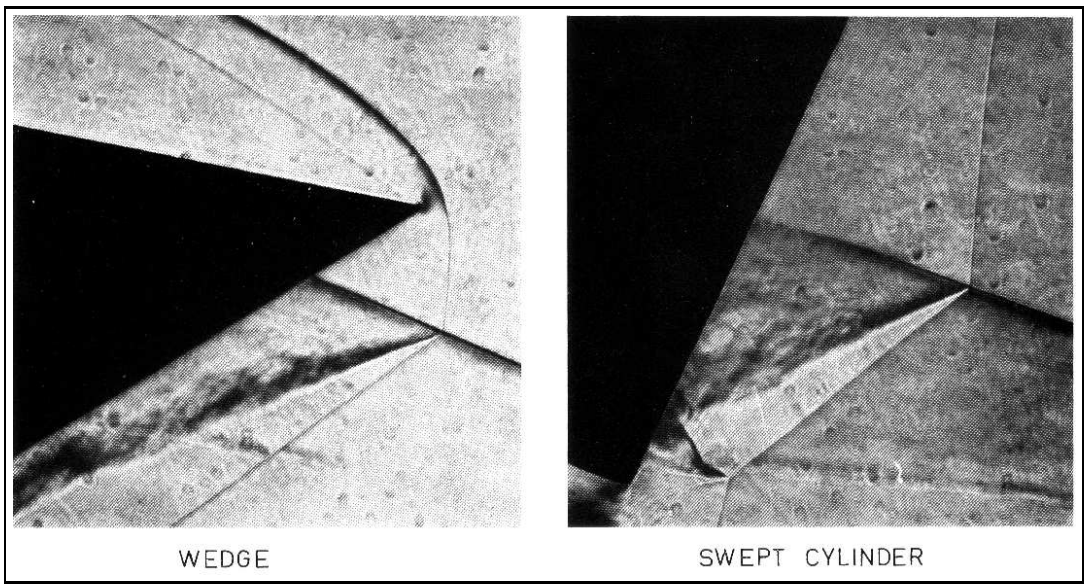

(b) Image from Edney's Experiment

Figure 9: Type III Interaction [4]

3.3.4 Type IV Interaction

The type IV interaction pattern is shown in Figure 10. This interaction pattern occurs when the impinging shock hits the body bow shock inside the subsonic region and the curvature of the body is such that the oblique shock PQ in the type III interaction is not possible. Generally a type IV interaction will occur when the impinging shock interacts with a normal shock created by the body in a region where the angle between the impinging shock and the body is large (on the order of 90°). The type IV interaction can increase local heating by over an order of magnitude. This is the most severe of the six interaction patterns and will be discussed in detail.

A characteristic feature of the type IV interaction is the strong, supersonic jet illustrated schematically by $RTUV$. In this region a shear layer is compressed and expanded repeatedly before terminating in a normal shock (line UV) that can lie *extremely* close to the body surface. What is interesting about this interaction is the series of oblique shocks, compressions, and expansions that processes the fluid in the shear layer will in general result in a significantly lower stagnation pressure loss than occurs though the other normal shocks in the interaction. Consequently fluid with a considerable amount of energy arrives at the body and is shocked by UV, further increasing its temperature. The point is that this particular interaction pattern allows for fluid with *much* more energy to arrive at the surface than an undisturbed normal shock would permit.

The analysis of this impingement is complicated by another factor: the exact width of the impinging layer depends strongly on the shock standoff distance associated with points P and Q. This is particularly important in computational approaches (CFD) in which shock wave resolution is difficult. Many CFD shock–capturing techniques (TVD, minmod, flux limiting, etc...) result in shock waves that are smeared over several grid points, but have the correct behavior in the control–volume sense that the average changes across the smeared wave are correct [16]. In the particular case of a type IV interaction smeared shock waves will result in substantial uncertainty in the size and strength of the impingement region. For computational approaches to be successful with these types of problems they must employ adaptive mesh refinement methods or other local solution enrichment techniques that can accurately resolve the shock waves. These approaches are generally considered to be research problems and have not found their way into many commercially available codes at this stage.

Another difficulty that Edney points out in the analysis of the type IV interaction is the presence of real gas effects in the hypersonic flight regime. It is known from perfect gas compressible flow theory that the maximum attainable density ratio across a normal shock wave is 6. However, as real gas effects become important this theoretical maximum disappears and density ratios significantly higher than 6 are realizable. This has the consequence of decreasing shock standoff distance since the gas behind a normal shock can be compressed more than in the perfect gas case. This has the important effect in the type IV interaction pattern of allowing the normal shock UV to move closer to the body, which may further

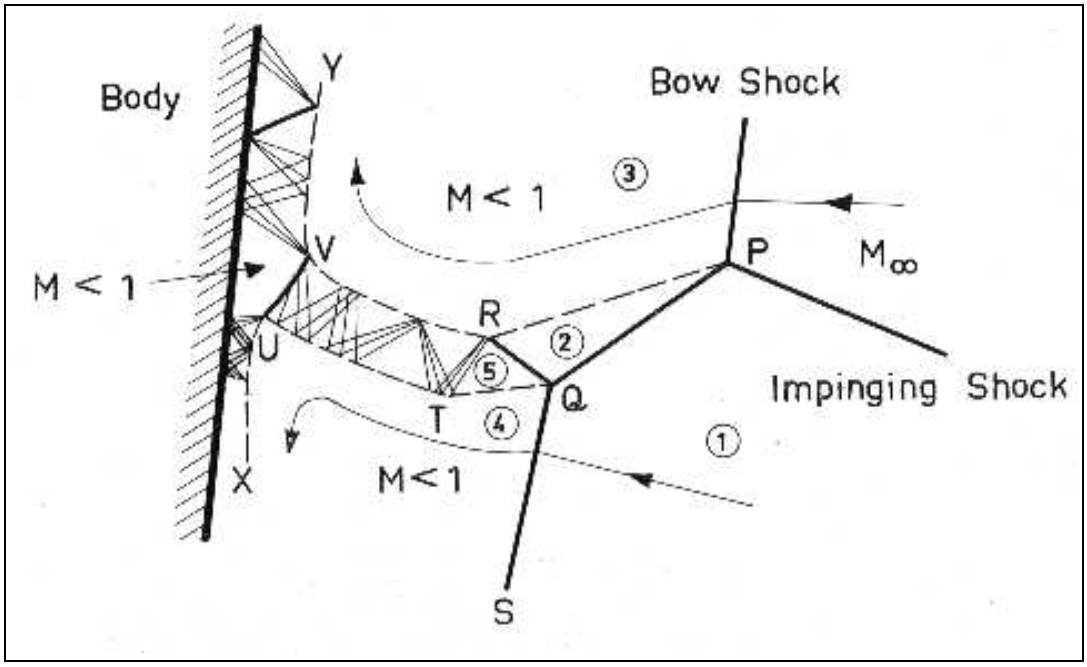

(a) Schematic Diagram

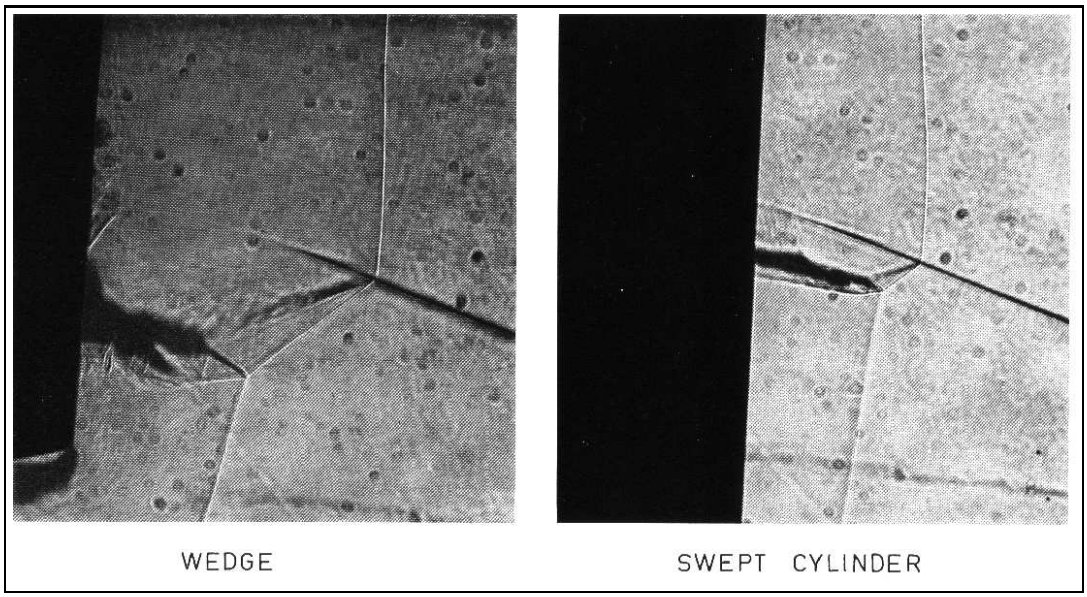

(b) Image from Edney's Experiment

Figure 10: Type IV Interaction [4]

compress the boundary layer and increase the heating rate. Also, in the case of non–equilibrium flow, it is fairly obvious that a strongly reacting gas will be in contact with the vehicle surface after it is processed by the normal shock UV. This further complicates the accurate prediction type IV interaction patterns by both experimental and computational methods in the hypersonic regime.

Figure 11 illustrates the ratio of peak pressure P_{60} produced by a type IV interaction to the otherwise undisturbed pressure P_{20} that results in a flowfield in which SSI is not present. The plot on the left shows the effect of varying the freestream Mach number M_∞ for a fixed specific heat ratio $\gamma = 1.4$. This plot indicates that as the freestream Mach number is doubled from $M_\infty = 10$ to $M_\infty = 20$ the pressure ratio essentially doubles from 18 to approximately 36. The plot on the right, on the other hand, shows the influence that γ has on this

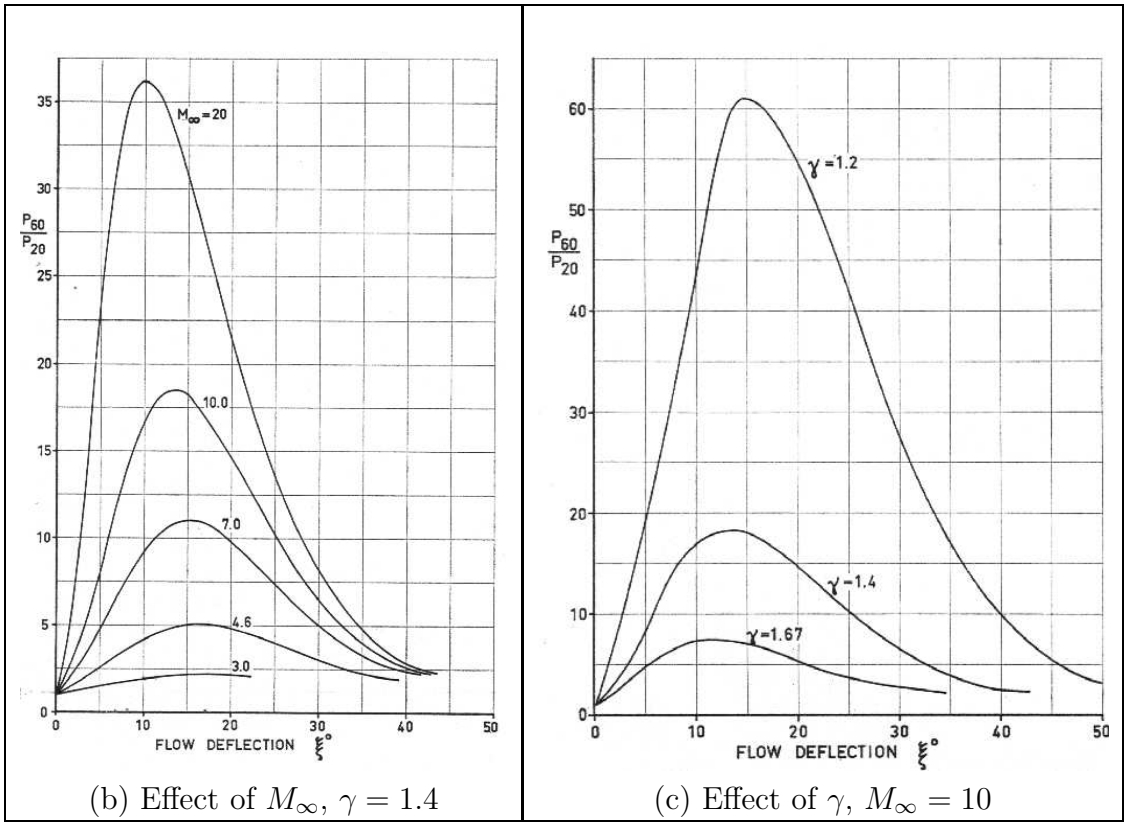

(b) Effect of M_∞, $\gamma = 1.4$ (c) Effect of γ, $M_\infty = 10$

Figure 11: The effect of M_∞ and γ on the pressure ratio across a type IV interaction pattern for a range of flow deflection angles [4]

pressure ratio for a fixed freestream Mach number $M_\infty = 10$. What is interesting about this plot is that as the ratio of specific heats drops from $\gamma = 1.4$ to $\gamma = 1.2$ the pressure ratio increases from approximately 18 to over 60! It is evident from this figure that the variation of γ has a much greater impact on the resulting interaction flowfield than even the freestream Mach number. This point clearly illustrates the importance of real gas effects in a type IV interaction. Ignoring real gas effects in hypersonic type IV interactions will cause any resulting analysis to be completely wrong.

3.3.5 Type V Interaction

The type V interaction pattern is shown in Figure 12. This interaction pattern results when the impinging shock meets the bow shock just above its upper sonic line. A characteristic feature of the type V interaction pattern is the strong jet that emanates from point P. In fact, except for the replacement of the shear layer with a much thinner jet, the type V interaction pattern is analogous to the type III pattern.

Since the fluid contained in the jet is processed the strong shock wave PQ it will have suffered a large stagnation pressure drop. This reduces the effect this jet will have on the body considerably compared to the type IV interaction. Additionally, the jet will in general interact with the body far downstream of the interaction region and will thus have time to diffuse some.

The shock QR, on the other hand, will impact the body in the vicinity of the interaction region. Much like in the type III case this shock can be sufficiently strong to induce boundary layer separation or transition. The state of the boundary layer on the body can thus change as a result of this interaction pattern and should be considered in analysis [4].

3.3.6 Type VI Interaction

The type VI interaction pattern is shown in Figure 13. This interaction pattern results when the impinging shock meets the bow shock well above its upper sonic line. A characteristic feature of this interaction pattern is the expansion fan between regions 2 and 4. Additionally, there is a shear layer that results from this interaction pattern. Both the expansion region and shear layer may impact the body downstream of the interaction region. However, it is notable that these features have not been observed to appreciably effect the surface heating [4].

It is interesting to note that prior to Edney's work only the type I and type VI interaction patterns had been reported in the literature. Since both of these patterns are fairly benign it is understandable that the importance of SSI was not fully realized until observed experimentally in the case of the X-15. Edney's work was critical in illustrating the importance of SSI effects in hypersonic aerodynamics.

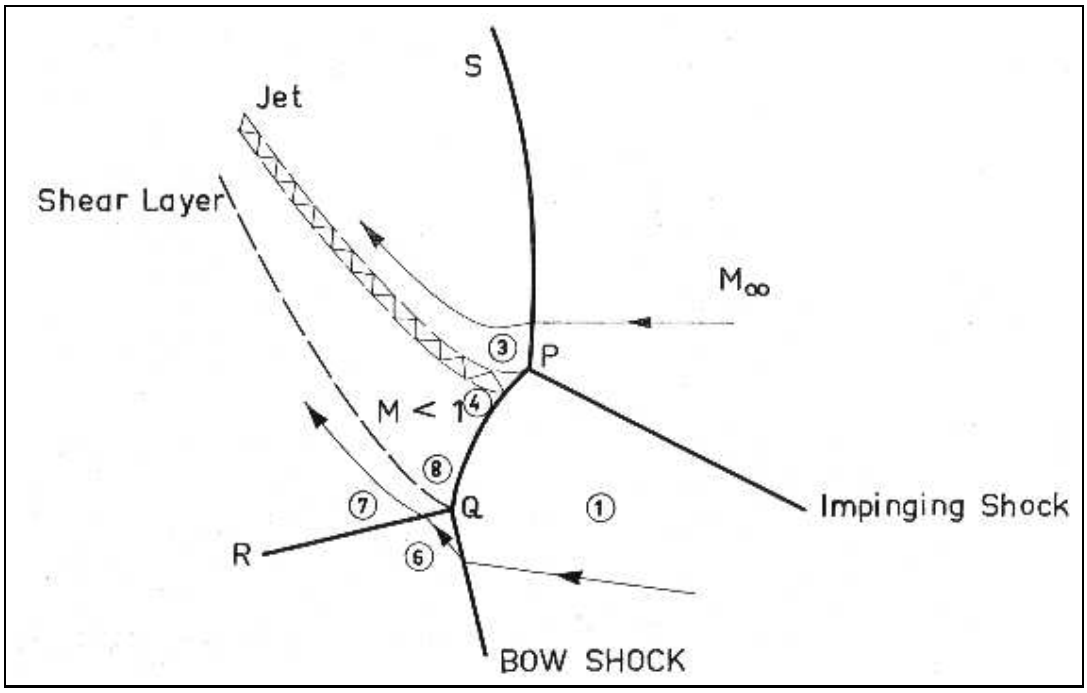

(a) Schematic Diagram

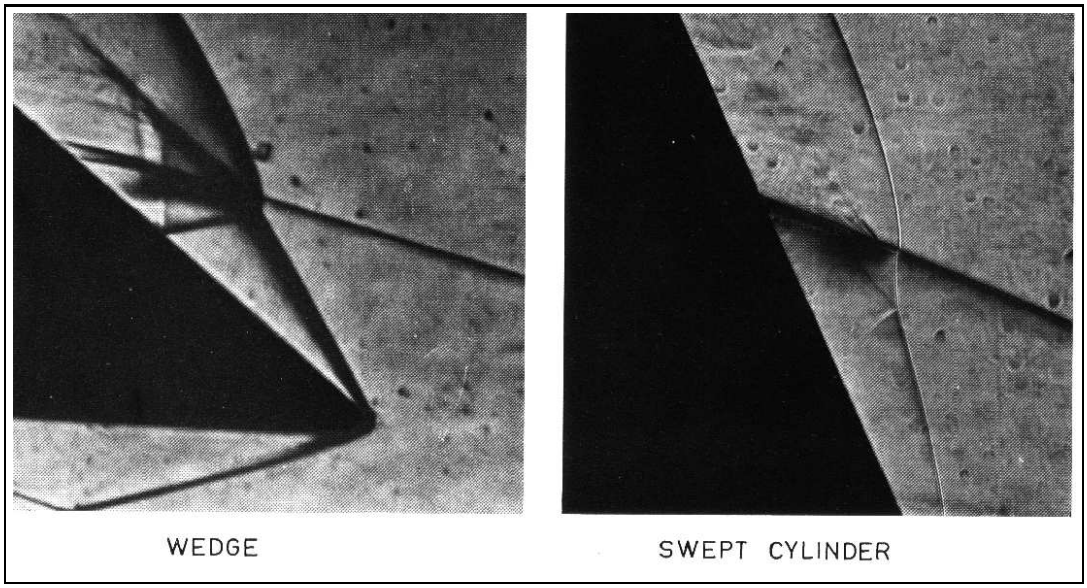

(b) Image from Edney's Experiment

Figure 12: Type V Interaction [4]

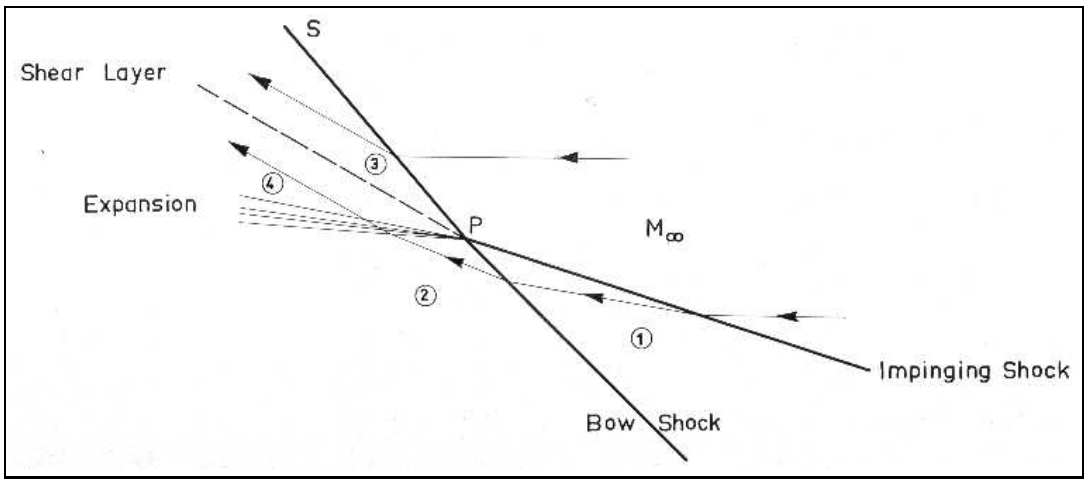

(a) Schematic Diagram

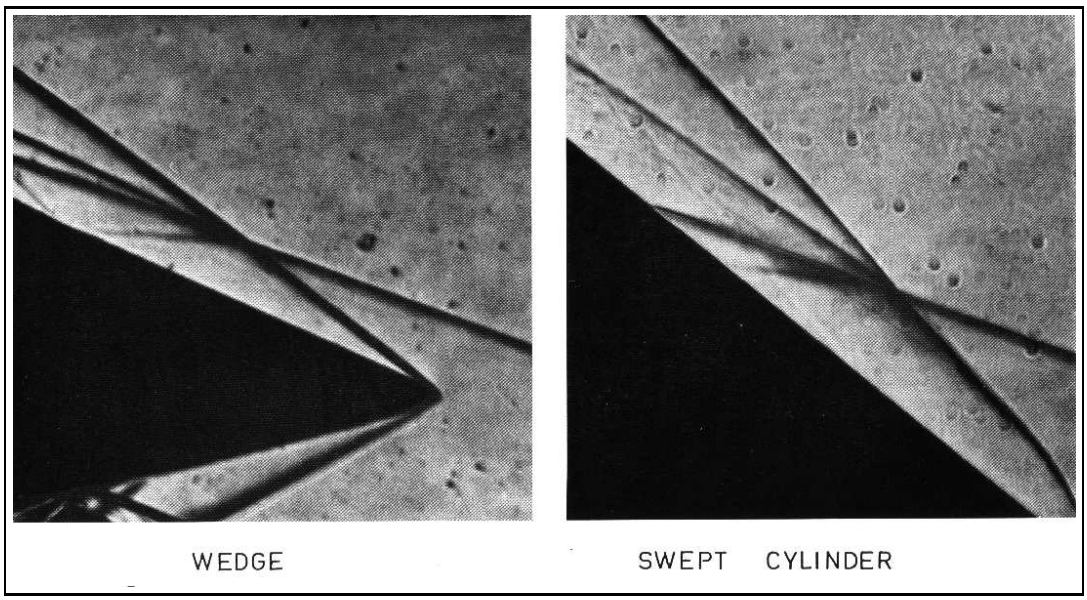

(b) Image from Edney's Experiment

Figure 13: Type VI Interaction [4]

4 Modern Research Techniques

The hypersonic SSI phenomenon is still very much a research problem. In the hypersonic regime the flowfield that develops external to a vehicle is critically influenced by real gas effects, boundary layer transition, and turbulent flow. Compared to other phenomenon in fluid mechanics these processes are not well understood and difficult to account for in both computational simulations and ground–based experiments. A general consensus in the hypersonic community seems to be that many of the open questions related to hypersonic flow can only be answered through flight tests. However, this situation presents a catch–22 since engineers must use computational tools and ground–based experimental techniques when designing flight test vehicles.

4.1 Experimental Techniques

Wind tunnels, shock tubes, and arc-jet facilities all provide an experimental environment in which hypersonic flowfields can be created. NASA's Langley Research Center (LaRC) has a number of tunnels that create Mach 6 to Mach 20 flow. [17] The Mach 20 tunnel in particular uses nitrogen as the test fluid. It seems obvious that reproducing proper real gas effects in a nitrogen flow will be impossible.

The H2K facility is a hypersonic wind tunnel located in Köln, Germany. Figure 14 depicts the tunnel with its test section open. Careful inspection of the

Figure 14: The H2K hypersonic wind tunnel in Köln, Germany [5]

figure reveals a model of NASA's X-38 prototype crew return vehicle in the test section. This tunnel, which is capable of operating from Mach 5 to Mach 11 for 30 seconds at a time, was used extensively in studying the high–speed aerodynamic behavior of the X-38. The maximum Reynolds number achievable in this tunnel is $20 \cdot 10^6$ per meter. To operate at peak conditions this tunnel requires 5 MW of power for a 30 second run. The tunnel typically runs 10 tests a day. [5]

A number of shock tunnel facilities are also operational. In these facilities the hypersonic flowfield around a test model is produced by a shock wave traveling though the test section. A number of variations of this principle are employed in practice, however the general approach is the same. An interesting feature of these facilities is the *extremely* short test durations. Typical run times are on the order of $100\mu s$. In such facilities measurements can become extremely complicated because techniques must be used that can respond fast enough to provide meaningful results before the test is over.

In general, experimental measurement of skin–friction and heat–transfer coefficients in hypersonic flow is extremely difficult. One reason for this difficulty is that it is difficult to seed hypersonic flow with particles that allow visual and laser–diagnostic techniques to be used. Another source of the difficulty is that proper shear stress measurements can be very complicated in turbulent boundary layers. This has the unfortunate effect of complicating the study of SSI in hypersonic flowfields. In such flowfields extremely high, localized heat fluxes can occur that must be accurately measured.

4.2 Computational Techniques

Over the past two decades computational power has increased at an amazing rate. With this rapid increase in computational power has come new techniques for analyzing problems in fluid mechanics. Computational fluid dynamics (CFD) is an approach in which a particular body of interest is modeled computationally and the governing equations of fluid mechanics are solved numerically [18, 19]. However, even today the prospect of a time–dependent flow calculation about a complicated three–dimensional body using the full Navier–Stokes equations is a daunting task. To help reduce the computational overhead associated with solving the complete Navier–Stokes set analysts often make simplifying assumptions that reduce the complexity of the governing equations. Some of these assumptions include:

- Inviscid flow. This assumption yields the Euler equations, which can be solved fairly easily with modern techniques. This approach does not allow for the computation of viscous effects like shear stress or surface heat transfer. Additionally, since hypersonic flowfields are often characterized by large shear layers this approach will not produce correct results for these cases.
- Perfect Gas. This assumption can be used to close the Navier–Stokes set (or a subset like the Euler equations) by providing an equation of state. However, this approach is invalid in the hypersonic regime when real gas

effects become important.

- "Thin–Layer" Navier–Stokes. In this approach the velocity derivatives parallel to the surface of the body are dropped from the governing equations. This approach is motivated by an order–of–magnitude analysis of the governing equations. However, it has the unfortunate consequence of not being able to compute separating flows correctly since many mechanisms for separation are removed.
- "Parabolized" Navier–Stokes. This is an interesting approach in which only the velocity gradients aligned with the flow direction are retained in the shear terms of the Navier–Stokes equations. This results in a parabolic PDE system that is in general easier to solve than the non–simplified equations which form a mixed hyperbolic–parabolic set. A drawback to this approach is that cross-flow instabilities and separation cannot be modeled correctly [16].

The CFD analyst considering hypersonic flow is thus left with a daunting task: she must solve the full Navier–Stokes equations around an arbitrary three–dimensional body *and* account for real gas effects. Equilibrium chemistry can be readily handled through table–lookup routines and other techniques, however in the case of chemical and thermal non–equilibrium the gas dynamics must be computed as part of the solution [18]. This is further complicated by the fact that many of the reaction parameters necessary to handle chemical non–equilibrium are not known to high accuracy. This is unfortunate, since as already discussed the influence of real gas effects in SSI flowfields can have a profound effect on the resulting heating environment. This influence is illustrated in Figure 15. The image on the left depicts Mach contours computed for a classic type IV

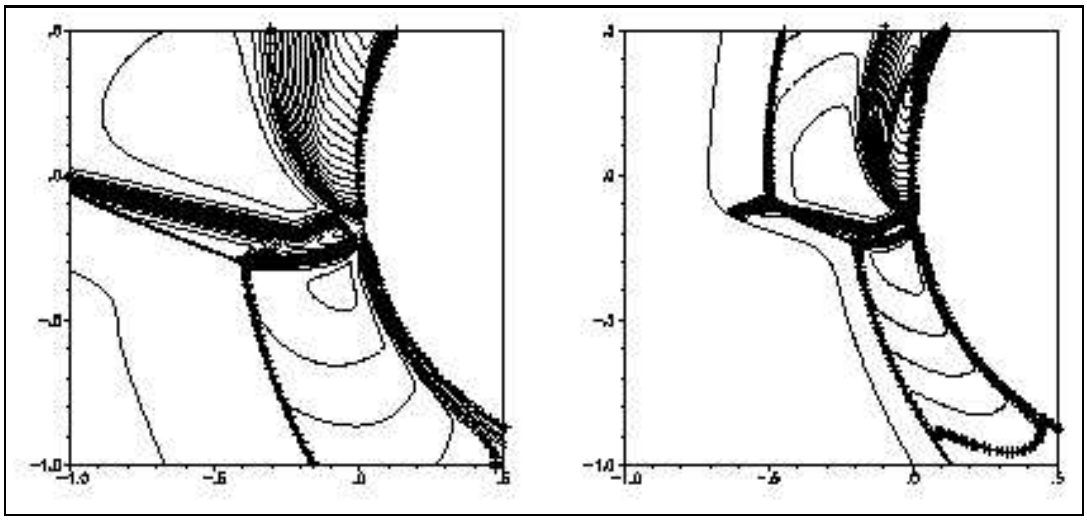

Figure 15: Mach contours computed in a type IV interaction [6]

interaction pattern with a perfect gas chemistry model. The image on the right is the same simulation with equilibrium chemistry. The resulting flowfields are

markedly different in these two cases.

Another difficulty that plagues CFD analysis in this class of problems is the accurate prediction of boundary layer/shear layer transition and the modeling of turbulent flow. The only way to currently predict transition is to use the approach of direct numerical simulation (DNS). In this approach the flow features are resolved to such a fine scale that the turbulent boundary layer and its structures are accurately computed. This technique is extremely computationally intensive and to date has only been applied successfully for simple geometries at very low Reynolds numbers. Additionally, many of the features such as surface roughness and vehicle vibration that actually induce transition are not adequately modeled, so any transition location predicted by DNS techniques is unreliable at best.

Even if the flow is fully turbulent CFD has a difficult time accurately modeling the effect of the turbulent boundary layer. Large–eddy simulation (LES) is a common technique in which large–scale turbulent structures are computed, and unresolved small–scale structures are modeled. However, the proper models to employ in LES simulations is still very much a research topic. The popular Smagorinsky model [20] and others currently produce reasonable results for a small range of flowfields, but a generally applicable model is not yet available. This has the unfortunate consequence of making computational prediction of boundary layer phenomenon like shear stress and heat transfer to be unreliable. It was noted earlier that in many SSI patterns the state of the resulting shear layers (laminar or turbulent) can have a significant impact on SSI–induced heat loads. Unfortunately modern CFD does not allow us to address this issue in a robust way.

Finally, another difficulty in using CFD techniques to compute SSI patterns is shock wave resolution. Modern techniques model the presence of a shock wave by smearing a large gradient over several computational cells [16]. This approach produces the correct behavior in a control–volume sense, but does not accurately predict the structure and *exact* location of the shock wave. Both of these parameters are crucial in the accurate computation of SSI patterns [4]. In order to accurately resolve the interacting shocks CFD codes must employ adaptive refinement techniques or other local solution enrichment strategies. These approaches are quite common in research codes, but are generally not available in commercial CFD codes.

5 The Significance of SSI in Hypersonic Vehicle Design

As mentioned in previous sections localized heat loads can be extremely severe in the case of SSI. This is particularly the case in the type IV interaction where peak heat loads can be up to *25 times* higher than undisturbed values [4, 6]. Obviously, it is critical to account for these interactions in hypersonic vehicle design. It is interesting to note that as vehicles and mission profiles become more

complicated the importance of predicting SSI effects becomes even more critical. This fact will be illustrated in the following sections first by examining hypersonic vehicles on which we currently have flight data and then by considering the importance of SSI effects on vehicles currently on the drawing board.

5.1 SSI Effects on Existing Hypersonic Vehicles

5.1.1 The Early Days of Manned Spaceflight

In examining the vehicles NASA has flown over the past 50 years we note that prior to the X-15 (whose SSI effects were considered in Section 2) there were no vehicles that exhibited important SSI effects. When considering the manned spaceflight program this seems to be a natural consequence of the mission profiles: rocket–assisted takeoff, orbit, and a ballistic, blunt–body reentry trajectory.

The Mercury, Gemini, and Apollo programs all employed capsule–type spacecraft with extremely blunt heat shields. Figure 16 shows the heat shield on a Mercury capsule after reentry. A characteristic feature of these early spacecraft

Figure 16: Mercury capsule heat shield after reentry [2]

was an extremely blunt heat shield. These heat shields protected the vehicle by helping reduce the convective heat transfer to the wall, since it is known that the wall heat flux decreases with increasing nose radius for a blunt body [21]. Additionally, these early vehicles were designed to have very low lift–to–drag (L/D)

ratios. Since they were not actively trying to control their trajectory during reentry control surfaces were also absent. Many of the features on more complicated vehicles were absent from these early designs, and it is often these features that cause SSI to occur.

5.1.2 The Space Shuttle Orbiter

The Space Shuttle Orbiter is the first vehicle in the manned spaceflight program in which SSI played an important role in its design. Figure 17 depicts the heating environment on the Orbiter surface at the time of peak heating in laminar flow. The heat flux magnitude is normalized by the heat flux that would

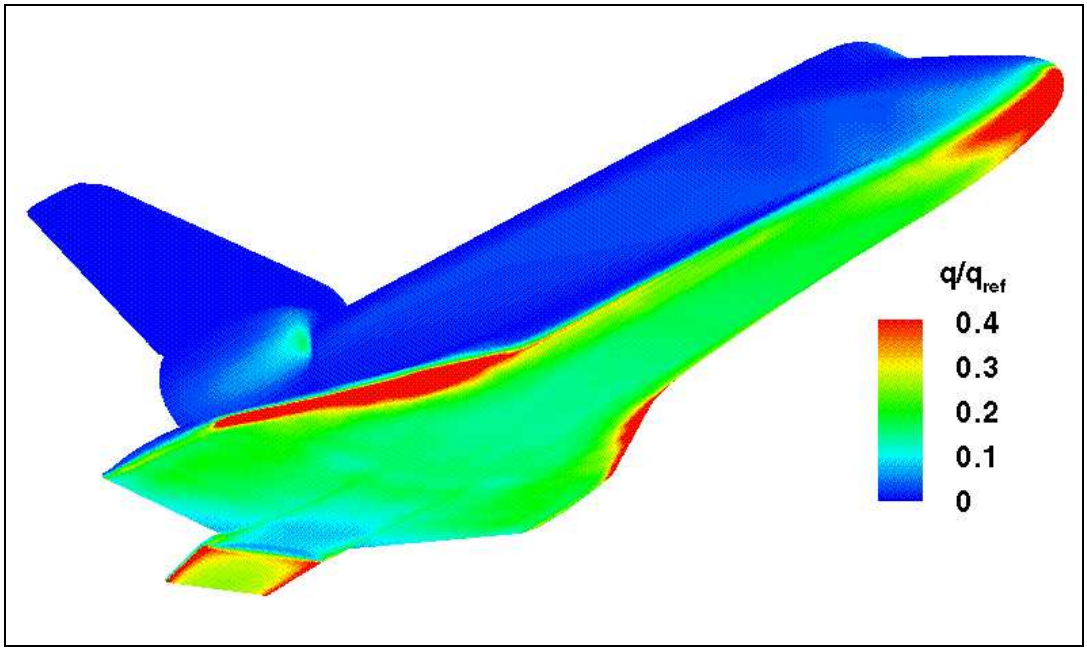

Figure 17: Orbiter surface heat flux for laminar flow [7]

result for a sphere of identical nose radius. What is interesting about the Orbiter is that the peak heating does not occur at the nose of the vehicle, which is what conventional wisdom might suggest. The peak heating actually occurs on the leading edges of the wings where the bow shock and wing shock interact. Figure 18 schematically illustrates this interaction region and suggests that it results in a classic type IV pattern. This type of interaction pattern seems quite reasonable since the bow shock will be impinging on the leading edge of the wing in the subsonic region of the wing shock.

The consequence of SSI in the case of the Orbiter is to limit the curvature of the leading edges and to demand increased thermal protection (TPS) on the leading edge of the wing. In fact, the nose and leading edges of the Orbiter are the only place where reinforced–carbon–carbon (RCC) is required to withstand the aerodynamic heating loads. The leading edges of the wings are also required to be relatively blunt because of this interaction. If the leading edges were sharper higher nominal heating rates would occur and the maximum heat flux resulting

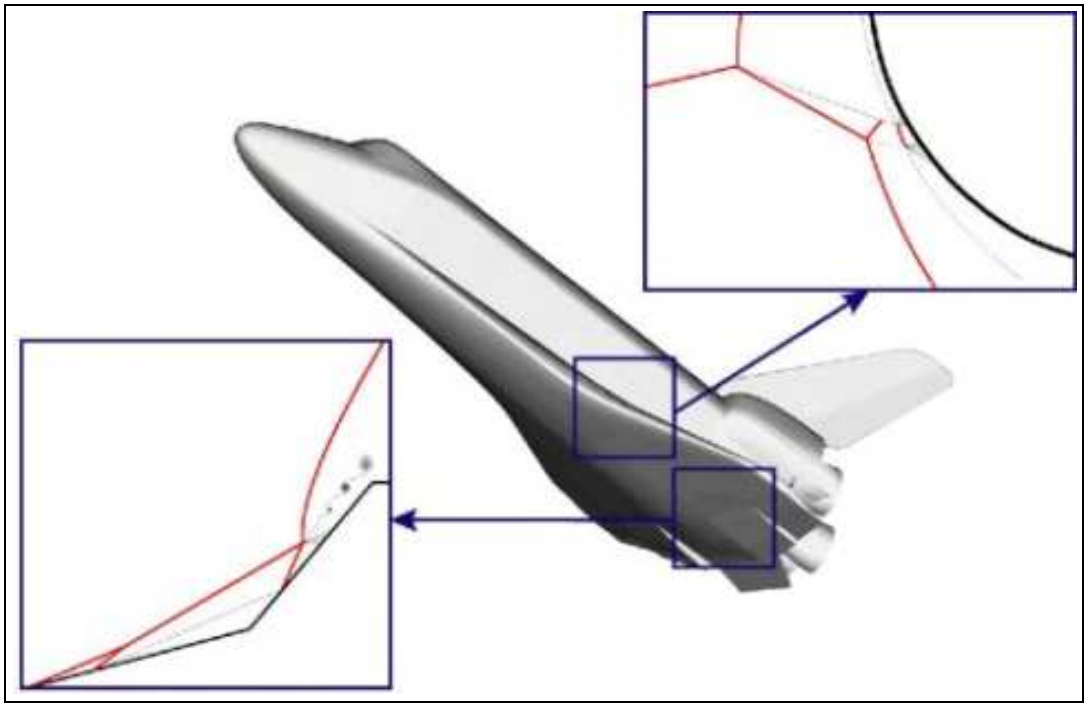

Figure 18: Schematic representation of the Orbiter bow shock/wing shock interaction

from the interaction would be even higher. This will become increasingly important as we look at modern designs that attempt to use air–breathing propulsion systems in the hypersonic regime. Such craft will demand more aerodynamic configurations, which will call for sharper leading edges and thus increase the significance of SSI effects.

5.2 The Increasing Importance of SSI Effects on Future Hypersonic Vehicles

Taking a look at the modern X-vehicle program illustrates that the focus of today's designs is on low cost, high performance, and reusability. The aerospace industry seems to be obsessed with reusable launch vehicles (RLVs) and single stage to orbit spacecraft (SSTOs) in an attempt to reduce the cost of space launch from approximately $10,000 to $1,000 per pound through more efficient designs. A close look at the design requirements for these next–generation vehicles illustrates that the importance of SSI effects will only become more significant in the immediate future.

5.2.1 The Expanding Flight Envelope

A consequence of SSTO flight may be that air–breathing propulsion systems are required. This is because the traditional spaceflight model of disposable rockets is quite expensive. Rockets are required to carry their own fuel *and* oxidizer,

which adds a significant amount of weight to the launch vehicle from both the oxidizer itself and the additional structure necessary to contain it. A consequence of this is that the total payload fraction a rocket is capable of carrying to orbit is extremely low. For example, only 1.5% of the Space Shuttle's takeoff weight is devoted to payload. For comparison, 32% of Boeing's 747 takeoff weight is devoted to payload.

In order to achieve the desired order–of–magnitude decrease in launch cost it may be necessary to abandon the rocket approach. The development of scramjet engines and other high–speed, air–breathing propulsion systems is identified as an enabling technology that may facilitate this dramatic decrease in launch cost. By taking advantage of the oxygen in the Earth's atmosphere these vehicles are only required to carry fuel (and not oxidizer), and thus could be much more efficient. A consequence of this approach, however, is that next–generation vehicles will be required to fly faster at lower altitudes (where more oxygen is available) than ever before [22]. In fact, this seems to be the case for SSTO–type vehicles regardless of what propulsion system is used.

Figure 19 depicts the flight envelope (the shaded region) in which an air–breathing hypersonic vehicle may operate. The figure also shows the Space Shuttle ascent and reentry trajectories for comparison. This figure clearly il-

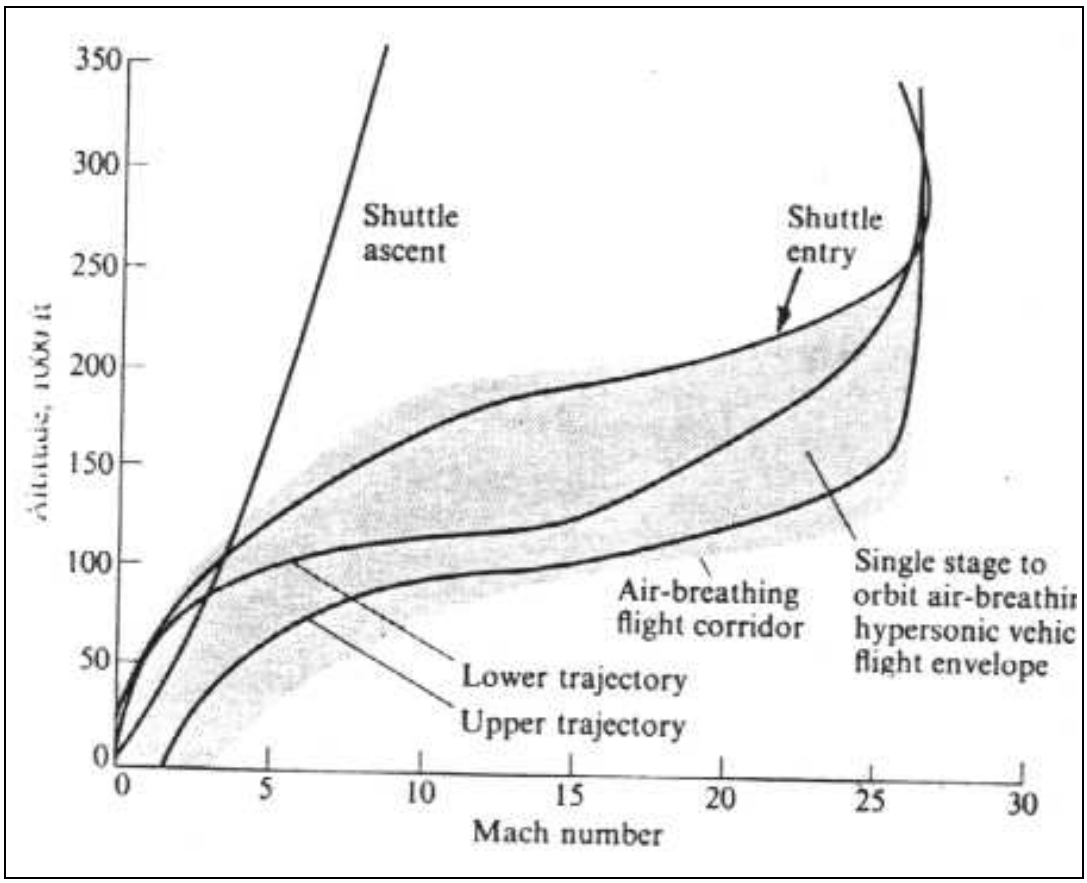

Figure 19: The expanding flight envelope for SSTO spacecraft

lustrates why SSI is becoming more important as we move away from the rocket approach. The Shuttle ascent trajectory (and other rockets in general) shows that by the time it enters the hypersonic regime it is at significant altitude. This has the effect of lowering the freestream density and minimizing the importance of aerothermodynamic effects like SSI.

What is interesting about the SSTO fight envelope is that it is much more varied than in the case of the Shuttle. Since the SSTO will require significant amounts of oxygen to feed its air–breathing engine we see that it must be capable of much higher speeds at lower altitudes than the Shuttle. We thus expect that aerodynamic effects (and SSI in particular) will become increasingly important in the design of these vehicles.

Figure 20 shows NASA's X-43, an experimental scramjet test vehicle. This

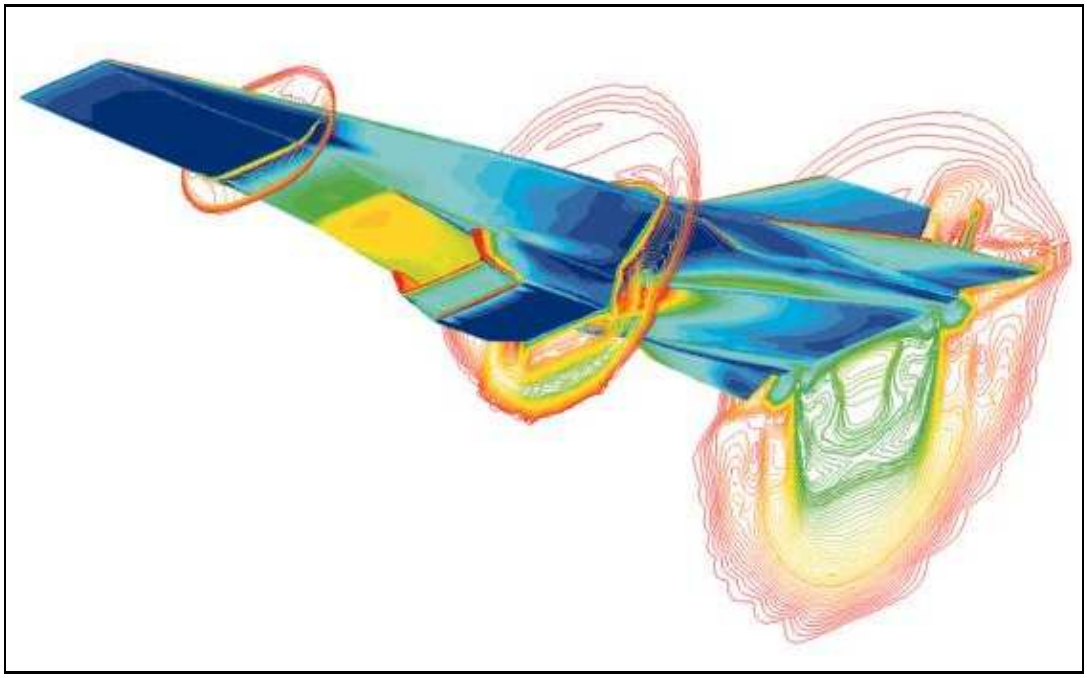

Figure 20: CFD prediction of Mach contours and pressure distribution around NASA's X-43 [2]

vehicle has many of the characteristic features of today's X–vehicles. Since it will require oxygen to feed its scramjet engine it must operate at an altitude where aerodynamic effects will be significant. This has the effect of requiring sharp leading edges on the nose, wings, tail, and engine inlet for this vehicle. Remember that in the case of the Orbiter the effect of SSI was mitigated by blunting the leading edges of the wings, since an increased radius of curvature results in lower convective heating. Since these next–generation vehicles will operate at lower altitudes for significant periods of time they must be extremely aerodynamic. Therefore they will require sharp leading edges and other features characteristic of high L/D vehicles. As a direct consequence, even undisturbed surface heating environments will be severe. The effect of SSI is then to increase these heating rates even higher, and clearly this must be accounted for in vehicle

design. If these effects are not considered catastrophic vehicle failure may result due to, for example, wing or tail burn–through and loss of vehicle control.

5.2.2 The Importance of Off–Design Flight Conditions

Another important aspect of RLV and SSTO flight vehicles is the importance of off–design conditions that the vehicle may be subjected to. The Space Shuttle reentry trajectory is very sensitive: if the Orbiter entry flightpath is too steep it will burn up, if its too shallow the vehicle will skip out of the atmosphere. These sensitive entry profiles are typical of unpowered reentry craft. A result of this sensitivity is that the designers know fairly accurately what the peak loads the craft will be subjected to are and can modify the design accordingly. Little variation from these design conditions is possible.

Things are different in the case of SSTO flight vehicles. Consider a manned, air–breathing scramjet vehicle for example. If the vehicle is operating at known speed and altitude engineers may be able to predict any important SSI effects on the vehicle and design its TPS accordingly. However, if the vehicle suffers an engine failure for some reason it will immediately decelerate and will be forced to land. It may then take an unpredictable flight path through a wide range of freestream conditions as it attempts to land. The vehicle must be able to withstand not only any severe, SSI–induced heat loads when everything is functioning normally, but also other severe heat loads that will occur in the off–design case.

The design engineers are now presented with a daunting task: develop a hypersonic flight vehicle and design its TPS so that it can withstand severe SSI–induced heating environments for a given flight profile. Then ensure that the design will survive a wide range of off–design conditions it may be subjected to. Additionally, this all must be done without over–designing the vehicle in such a way that it is too heavy to be practical or cost–effective.

5.2.3 The Role of TPS in Next–Generation Vehicle Design

The need for a robust thermal protection system on these next–generation vehicles should now be apparent. These vehicles must withstand harsh heating environments for a range of unpredictable flight profiles. Additionally, the vehicles themselves must be extremely lightweight so that they can carry a meaningful payload. Finally, any TPS on these vehicles must be robust, require little maintenance, and last for many missions in order to be truly reusable.

It is clear that existing TPS technologies such as Apollo's ablative heat shield and the Space Shuttle's ceramic tiles are not up to the job. Figure 21 shows ground crews baking the Orbiter Atlantis's tiles under heat lamps in an attempt to dry them out. Atlantis landed in the rain at Edwards Air Force Base, and flight engineers worried that any moisture between the tiles would freeze, expand, and thus cause tiles to separate once in the chilly vacuum of space. This drying process actually caused a subsequent launch to be delayed. Clearly the TPS employed in any robust, reusable next–generation vehicle must be insensitive to

Figure 21: Atlantis sunbathing after landing in the rain. Image courtesy of the Houston Chronicle.

conditions such as rain.

A possible solution may be found in the "3^{rd} generation" TPS currently under development at NASA's Ames research center. The new systems employ ultra–high temperature ceramic (UHTC) materials that can withstand significant heat loads without ablating [23]. Initial results indicate that UHTC may be useful on future hypersonic vehicles, thus protecting these vehicles from the extreme heat loads produced by the combination of SSI and sharp leading edges. However, these materials are still very much in the design phase.

It is clear that the development of new hypersonic vehicles will require advanced materials. The flowfields around these vehicles will be complicated by SSI interaction patterns that can increase already severe heating environments by an order of magnitude or more. Furthermore, these vehicles must be designed to survive unpredictable flight paths in the hypersonic regime that could result from subsystem failure.

6 Conclusions

Shock–shock interaction (SSI) is an important consequence of supersonic flight. In the supersonic regime complex bodies may create multiple shock waves that can interact with each other. It is interesting that there was little experimental investigation of the SSI problem until the end of the 1960's. At this time a structural failure on NASA's X-25 rocket plane was attributed to SSI, and interest in the problem grew intensely.

Some of the first work in the field was done by Edney, who identified six distinct interaction patterns that can result from SSI. The conditions under which these patterns are established was also determined. Of the six patterns the most severe was found to be the type IV pattern, in which localized heating rates can easily surpass undisturbed values by an order of magnitude or more.

Modern computational and experimental techniques for investigating the SSI phenomenon are plagued by a number of problems. It is difficult to accurately measure heat transfer in localized interaction regions, particularly in the case of hypersonic flow. Additionally, shock wave resolution is critical in predicting the effects of SSI, so many computational techniques are unreliable. Finally, the presence of real gas effects as well as shear/boundary layer transition and turbulence are two difficult problems that make accurate simulation and experimental investigation of SSI extremely difficult.

Examining past and present hypersonic vehicles suggests that as trends in vehicle design emphasize reusability and reduced cost the importance of SSI effects become even more pronounced. In general, SSI effects can be expected to worsen with the introduction of high lift–to–drag ratio, air–breathing, single–stage–to–orbit flight vehicles. The difficulties associated with designing these vehicles is compounded by the need to consider an ever–increasing flight envelope and the complexity of dealing with off-design flight conditions. Advanced thermal protection systems must be developed that are capable of protecting these vehicles from severe SSI–induced heat loads over a wide range of flight conditions.

The influence of SSI on hypersonic vehicle design is found to be considerable. A vehicle that is not designed to withstand SSI effects will undoubtedly fail in the hypersonic regime. The importance of understanding SSI effects on vehicle design will only increase in the future as the aerospace industry seeks to create more efficient and reliable vehicles.

Acknowledgments

The author would like to thank the U.S. Department of Energy for supporting him through the Computational Science Graduate Fellowship while this research project was completed. He also thanks Dr. David Dolling for several discussions during the research phase and his help in outlining the scope of the project.

References

[1] John V. Becker, "The X-15 Program in Retrospect." http://www.hq.nasa.gov/office/pao/History/x15lect/toc.html.

[2] NASA Dryden Flight Research Center, "X-15 Photo Gallery." http://www.dfrc.nasa.gov/gallery/photo/X-15/, 2001.

[3] J. Armstrong, "Expanding the X-15 Envelope to Mach 6.7 – A Personal Account." http://www.edwards.af.mil/history/docs_html/aircraft/x-15_mach6.7.html, 2001.

[4] B. Edney, "Anomalous heat transfer and pressure distributions on blunt bodies at hypersonic speeds in the presence of an impinging shock," *FFA Report 115*, 1968.

[5] A. Henckels, "Hypersonic wind tunnel h2k." http://www.sm.go.dlr.de/SMinfo/WTKinfo/Windkanaele/H2K/H2K_Seite_e.html, June 2000.

[6] S. Brück, "Investigation of shock-shock interactions in hypersonic reentry flows." http://www.sm.go.dlr.de/štefan/paper/ISSW95/issw95.html, December 1997.

[7] NASA Langlet Research Center, "X-15 Photo Gallery." http://www.larc.nasa.gov/gallery/photo/X-15/, 2001.

[8] R. D. Banner, A. E. Kuhl, and R. D. Quinn, "Preliminary results of aerodynamic heating studies on the x-1.5 airplane." NASA TK x-638, March 1962.

[9] "North American X-15." http://users.dbscorp.net/jmustain/x15.htm.

[10] W. L. Francis, "Experimental heat–transfer study of shock impingement on fins in hypersonic flow," *Journal of Spacecraft and Rockets*, vol. 2, pp. 630–632, July–August 1965.

[11] R. Heirs and S. Loubsky, "Effects of shock–wave impingement on the heat transfer on a cylindrical leading edge," *NASA TN D-3859*, 1967.

[12] R. Newlander, "Effect of shock impingement on the distribution on heat–transfer coefficients on a right circular cylinder at mach numbers of 2.65, 3.51, and 4.44," *NASA TN D-642*, 1961.

[13] D. S. Dolling, "50 Years of Shock Wave/Boundary Layer Interaction – What Next?," in *Proceedings of the Fluids 2000 Conference*, (Denver, CO), American Institute of Aeronautics and Astronautics, June 2000.

[14] P. J. Finley, "Experiments on the reattachment of a turbulent axisymmetric shear layer," *Aerospace Quarterly*, vol. 18, pp. 379–398, November 1967.

[15] P. J. Baker and B. W. Martin, "Heat transfer in a supersonic separated flow over a two–dimensional backward–facing step," *International Journal of Heat and Mass Transfer*, vol. 9, pp. 1081–1088, October 1966.

[16] J. C. Tannehill, D. A. Anderson, and R. H. Pletcher, *Computational Fluid Mechanics and Heat Transfer, 2^{nd} ed.* Taylor & Francis, Washington, D.C., 1997.

[17] NASA, "Wind tunnels – nasa's wind tunnels." `http://observe.ivv.nasa.gov/nasa/aero/tunnel/tunnel_nasa.html`, 1999.

[18] J. D. Anderson, *Hypersonic and High Temperature Gasdynamics*. American Institute of Aeronautics and Astronautics, Inc., 2000.

[19] J. D. Anderson, *Modern Compressible Flow with Historical Perspective, 2^{nd} ed.* McGraw-Hill, 1990.

[20] S. K. Aliabadi and T. E. Tezduyar, "Parallel fluid dynamic computations in aerospacce applications," *International Journal for Numerical Methods in Fluids*, vol. 21, pp. 783–805, 1995.

[21] W. D. Hayes and R. F. Probstein, *Hypersonic Flow Theory*. Academic Press, New York, 1959.

[22] J. D. Mattingly, *Elements of Gas Turbine Propulsion*. McGraw-Hill, 1996.

[23] J. Salute, "Sharp: Slender hypervelocity aerothermodynamic research probes." `http://asm.arc.nasa.gov/projects/sharp/index.shtml`, May 1997.